ELSEVIER

Earth and Planetary Science Letters 126 (1994) 217–234

EPSL

Magnetic properties of the High Himalayan leucogranites: Structural implications

Pierre Rochette [a], Bruno Scaillet [b], Stéphane Guillot [c], Patrick Le Fort [c], Arnaud Pêcher [c]

[a] *CEREGE, case 431, Faculté St-Jérôme, 13397 Marseille Cedex 20, France*
[b] *CRSCM, 1A rue de la Férollerie, 45071 Orléans Cedex France*
[c] *Institut Dolomieu, 38000 Grenoble, France*

Received 29 October 1993; revision accepted 7 July 1994

Abstract

The magnetic properties of the High Himalayan leucogranites have been investigated on 527 specimens in three plutons, Everest–Makalu (6 sites) and Manaslu (40 sites) in Nepal, and Gangotri (43 sites) in India. Susceptibility varies between 2 and 100×10^{-6} SI, with an anisotropy ratio up to 1.16. High field and low-temperature magnetic measurements together with comparison with weight percent iron demonstrate that anisotropy of magnetic susceptibility is carried by paramagnetic biotite and tourmaline. The latter produces an inverse fabric, i.e. with the minimum axis parallel to mineral lineation. The magnetic fabric demonstrates complex patterns of stretching lineations during magmatic emplacement, and its usefulness in semi-quantitatively estimating petrofabric intensity is demonstrated for the biotite-bearing facies. Natural remanent magnetization was measurable at only two sites in Everest–Makalu, where there are well-defined reverse directions carried by titanomagnetite and pyrrhotite. Comparison of these preliminary results with predicted directions for stable India suggests northward tilting of about 10° and a small clockwise rotation of this massif.

1. Introduction

Leucogranitic plutons are found in practically all orogenic belts, as a result of syntectonic anatexis of the thickened continental crust. During emplacement their internal flow structures record in a complex fashion the tectonic regime of their solid environment and subsequent high-temperature ductile deformation. Therefore petrofabric studies in such granites have significant geodynamic implications. Anisotropy of magnetic susceptibility (AMS) is a major means of studying these petrofabrics because of sensitivity and rapid measurement. (For a general presentation of the technique see [1–3], and for applications to syntectonic anatectic granites see [4–6].) Rigid body rotations and latitudinal drift affecting the pluton after its solidification may also be studied by comparing the characteristic directions of natural remanent magnetization (NRM) with paleomagnetic directions predicted (e.g., [7]) or observed from stable cratonic areas [8,9]. The applications of both techniques is tested in this paper for the High Himalayan leucogranites. Special attention is paid to the characterization of the magnetic mineralogy, which is necessary for interpreting correctly the NRM and AMS data. This paper aims at presenting a synthesis of the magnetic

SSDI 0012-821X(94)00151-0

properties of the three plutons (Everest–Makalu and Manaslu in Nepal, and Gangotri in India) (Fig. 1a), together with mineralogical and structural applications of the AMS and NRM data in Everest–Makalu. The structural application of AMS in Gangotri and Manaslu is detailed in [10] and [11] respectively.

2. Geological setting

The High Himalayan leucogranites occur as a thin belt of discrete plutons with similar features. They were emplaced as kilometre-scale sheet-like intrusions within the sedimentary succession at the top of the Tibetan slab, above the Main Central Thrust (MCT), and at the southern border of the Tibetan plateau (Fig. 1a, after [12]). These leucogranites derived from the anatexis of stacked metamorphosed crustal slices during the late Tertiary. Radiometric ages range from about 25 to 15 Ma [12]. The deformation of the Himalayan range at this time was mainly characterized by northward underthrusting of India below the MCT, resulting in a pervasive schistosity and N–S stretching lineation within the overlying metamorphic rocks, although E–W lineations are also reported [13,14]. Above the granites extensional structures such as normal faults of clearly post-metamorphic age [15,18] and late–post-metamorphic folds [19,20] occur, and these are interpreted as being the the result of a northward collapse of the High Himalayan range. These structures are cut by the leucogranites in some places [10]. E–W dextral shear, which is indicated in the present-day kinematic situation by Quaternary N–S grabens and eastward extrusion of Tibet [21,22], has been demonstrated to have occurred during the Miocene in the upper part of the slab close to the level of granite emplacement [23,24]. It is therefore very important to place constraints on the flow structure of the granites, which are important indicators of the kinematic regime within the crust.

The petrological characteristics of the massifs are quite constant: A typical facies with tourmaline (up to 5%), muscovite (up to 10%) and sometimes garnet is generally encountered within the pluton, whereas a second facies, with biotite (up to 3%) instead of tourmaline, is more common at the border of the intrusion [25]. However, biotite and tourmaline are not mutually exclusive, and tourmaline–biotite-bearing facies are quite common. The emplacement temperature of these granites probably lies between 640°C (the water-saturated solidus) and 700–800°C (the liquidus temperature, which varies according to the water content and composition of the melt) [26].

3. Sampling

Due to the difficult access (most outcrops are above 4000 m and the highest, site B in Fig. 1b, is at 5600 m), the three studied plutons were sampled using blocks (one per outcrop, except in Everest) of about 1 kg oriented with the magnetic compass in the field. Between 3 and 8 cylindrical specimens of 10.8 cm^3 were drilled from each block in the laboratory. In the Gangotri–Badrinath massif in India (Fig. 1a) 43 blocks (197 specimens) were measured as a part of a thesis on the structural and petrological features of that massif [10]. In the Manaslu massif, 40 oriented blocks (279 specimens) from field collections were selected for magnetic study [11]. In the Everest–Makalu massif 11 blocks (51 specimens) from 6 outcrops (Fig. 1b, A–F) were collected during a specific expedition, during which great care was taken in field orientation by using a specially designed tripod. In the Everest area the granite outcrops on steep cliffs that begin over 4500 m above sea level. Therefore only the basal part of the massif was sampled, except at site A which is in a 20 m thick leucogranitic sill, below the main granitic body of Cho Oyu.

4. Laboratory techniques

4.1. Magnetic anisotropy

The AMS was measured in Grenoble using a KLY-2 susceptibility bridge manufactured by Geofizyka (Brno, Czech Republic). In the Everest leucogranite, both standard 10.8 cm^3 and large 65

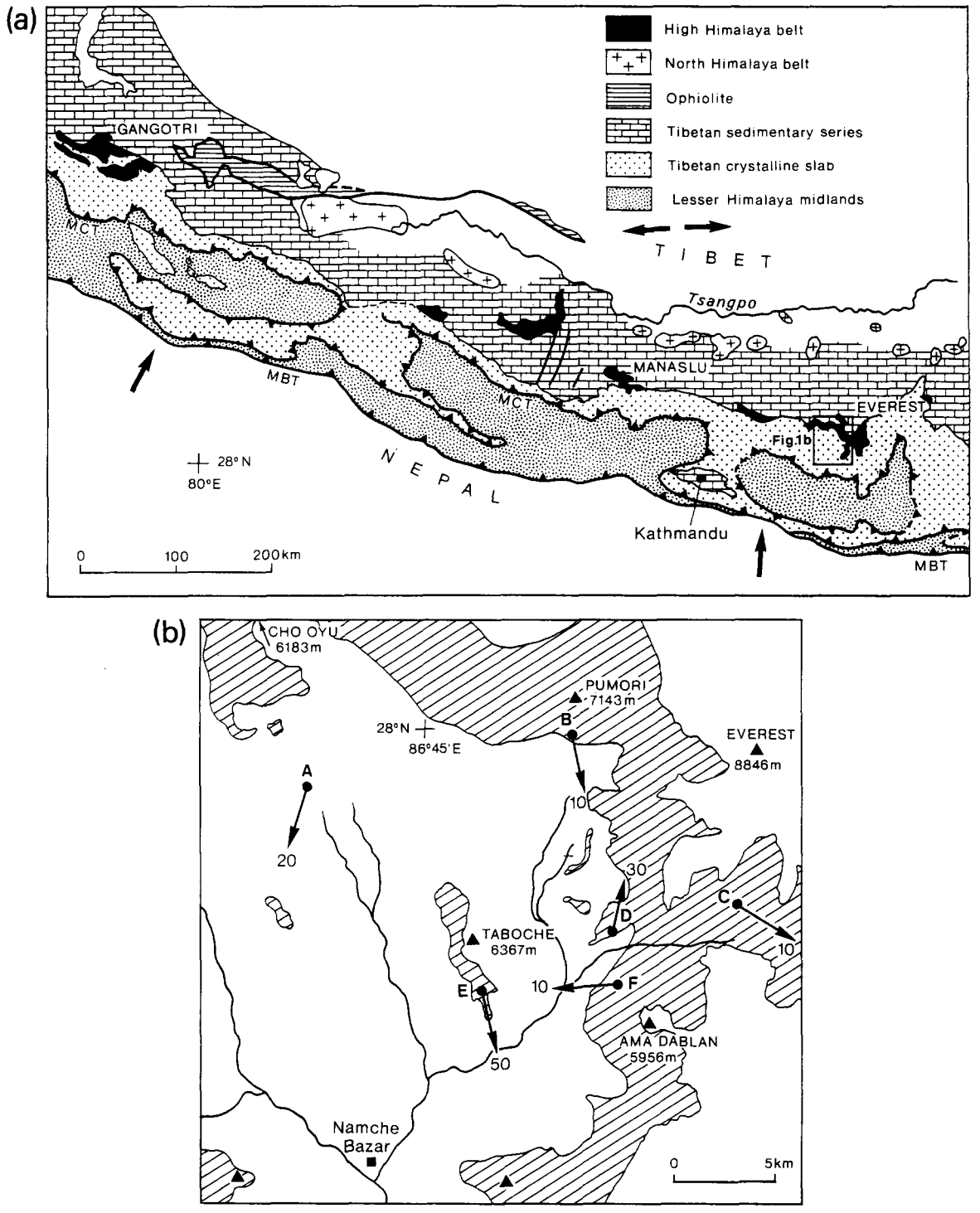

Fig. 1. (a) Geological sketch map of the Himalaya with the main lithological and structural features. The High Himalaya leucogranitic belt that bears the three studied massifs is shown in black. (b) Simplified map of the Everest granite (shaded area, after Vuichard, pers. commun.; see also [50]) with sampling sites A–F. Stretching lineation deduced from AMS measurements is shown with arrows with dip angles.

cm^3 samples were measured to investigate dispersion of the data due to the large grain size of the granite.

A sequence of 15 measurements of susceptibility along different axes was used to compute the susceptibility ellipsoid (whose principal axes are labelled $K_1 \geq K_2 \geq K_3$) and the confidence ellipses for these axes. Reported here are the anisotropy ratios including lineation ($L = K_1/K_2$), foliation ($F = K_2/K_3$) and anisotropy degree ($P = K_1/K_3$). The mean susceptibility is $K_m = (K_1 + K_2 + K_3)/3$ [1]. Using the KLY-2 bridge, sensitivity on K_m is 0.05×10^{-6} SI, whereas significant K_1 and K_3 directions may be obtained down to an anisotropy ratio of 1.002.

For each site, the K_1 and K_3 directions of all specimens are plotted on stereoplots, which also show structural foliation and lineation, if visible in the sample. Mean directions are computed using the tensorial mean statistics of Jelinek [27], which provide confidence ellipses around the mean directions and mean L and F values. Due to the very low K_m values in these granites a correction for the diamagnetic contribution D must be performed on L and F to obtain values independent of the amount of paramagnetic silicates and thus truly characteristic of the preferred orientation (see demonstration in [33]; ratios are derived from principal susceptibilities minus D).

To characterize the fabric of the NRM-carrying grains, the technique of anisotropy of anhysteretic susceptibility (AAS; e.g., [28]) was used in the Institute for Rock Magnetism in Minneapolis. The AAS ellipsoid was computed using a sequence of acquisition of anhysteretic remanence in a 0.1 mT bias field and a 100 mT AF field, along 9 different directions following the McCabe et al. [29] technique.

4.2. Remanence measurements and demagnetization

Standard NRM measurements following alternating fields and stepwise thermal demagnetizations were completed on the 10.8 cm^3 samples using either the Molspin spinner magnetometer in Grenoble or the ScT cryogenic magnetometer at the Lamont Doherty Geological Observatory. The type of NRM preserved in these rocks has been investigated by comparing the stability of NRM and a laboratory TRM vs. temperature for the same samples. The procedure, using a high-temperature measurement device developed by R. Dunn and M. Fuller at he University of California, Santa Barbara, provides very accurate measurements of remanence during heating and only a minor risk of alteration during the TRM experiment (see [30] for more complete description). The bias field used for TRM was 45 μT and the maximum temperature from which the sample was cooled in the bias field is taken at about 50°C higher than the maximum unblocking temperature determined during the first heating of NRM in a zero field.

4.3. Low-temperature and high field measurements

Other rock magnetic experiments were completed in Grenoble, including low-temperature analysis of induced and remanent magnetization using the high field SHE cryogenic magnetometer of the L. Néel Laboratory [31]. Pyrrhotite is a mineral that is often difficult to identify through rock magnetic parameters and a new and very specific method using a low-temperature transition at 34 K visible through cooling down to liquid helium temperature a room-temperature saturation isothermal remanent magnetization (IRM) has been proposed [32]. Magnetite can also be identified by this technique by its Verwey transition at 120 K. The SHE magnetometer is also used to compute high field susceptibility (K_{HF}) at room temperature on 1 cm^3 samples, and to compare with low field susceptibility at room temperature (K_{LF}) measured with the KLY-2 bridge on the same small samples. Low-temperature variation in K_{HF} can characterize the diamagnetic contribution (negative susceptibility, D, independent of temperature) and the paramagnetic contribution due to iron-bearing minerals such as ferromagnesian silicates. For this purpose $K_{HF}(T)$ may be fitted by the law:

$$D + C/(T - \theta) \quad (1)$$

where C is the Curie constant proportional to the amount of magnetic ions in the sample and θ is

the paramagnetic Curie temperature, which depends on the type and intensity of interactions between the magnetic ions [3]. For very dilute ions in the paramagnetic mineral, where interactions are negligible, $\theta = 0$ K.

4.4. Geochemistry and petrofabric

Analyses of major and some trace elements were performed on all the studied blocks using an ICP absorption emission spectrometer at CRPG Nancy. For a diamagnetic (assigned to the quartz value $D = -14.5 \times 10^{-6}$ SI; [1,3]) plus paramagnetic (due to iron-bearing minerals) mixture, with θ values negligible compared to 295 K, we can derive the following formula for volume susceptibility:

$$K_m = -14.5 + d(25.2t + 33.4t')10^{-6} \text{ SI} \qquad (2)$$

where d is the density of the rock, and t and t' are the weight percent of Fe^{2+} and Fe^{3+} ions respectively [33]. Total Fe_2O_3 has been analyzed for each block, and block mean 'volume' susceptibility is taken as the average of specimen mass susceptibility multiplied by a constant average density of 2.65.

The preferred orientation of phyllosilicates has been studied in some oriented thin sections using the image analyser system at Nancy [34].

5. Magnetic mineralogy of the High Himalayan leucogranites

5.1. Origin of magnetic susceptibility

Previous studies have shown that the susceptibility in anatectic granites is essentially dominated by paramagnetic silicates [6,33,35].

Low field magnetic susceptibility at room temperature (K_{LF}) is found in this study to vary from 2 to 100×10^{-6} SI, with higher values mainly in the Everest massif (K_{LF}–D values are reported in Fig. 2). Such low values are usually found when the ferromagnetic minerals make only a minor contribution to K_{LF} [33,35]. This can be checked quantitatively by comparing high field susceptibility at room temperature (K_{HF}) with K_{LF}. Such

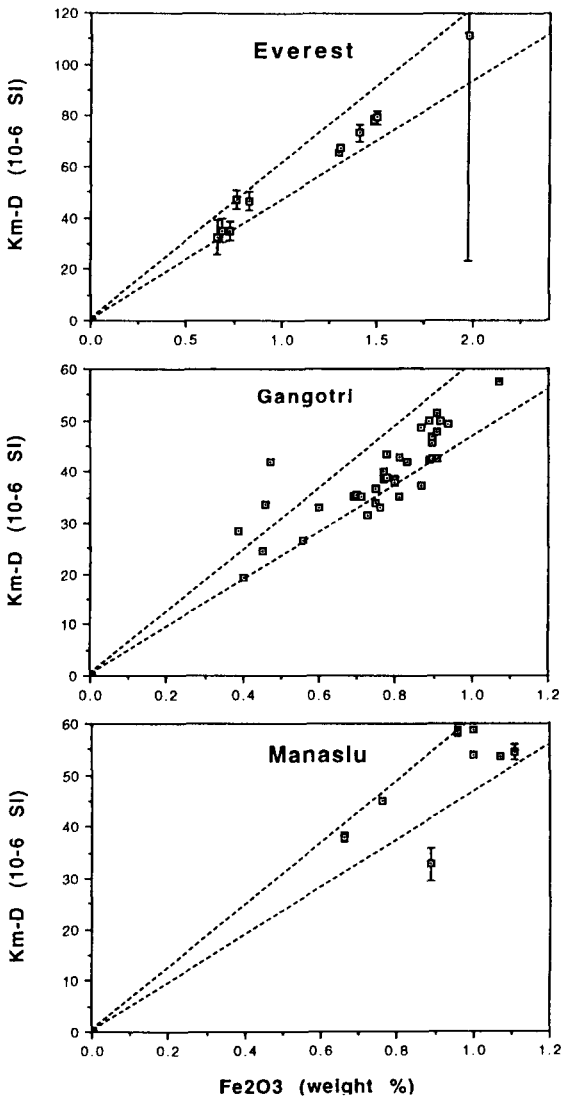

Fig. 2. Mean low field susceptibility K_m corrected from constant diamagnetic contribution vs. Fe_2O_3 content for the blocks analyzed in the three massifs. The error bars on K_m correspond to the standard deviation between specimens of the same block. The upper and lower dashed lines correspond to the theoretical curves for paramagnetic Fe^{2+} and Fe^{3+} respectively.

measurements [31] have been performed with the SHE susceptometer on 8 samples from the Gangotri and Everest granites (Fig. 3). The plot of K_{LF} vs. K_{HF} clearly demonstrates that ferromagnetic minerals make a negligible contribution to K_{LF}: all points (open symbols) fall on the $K_{LF} =$

K_{HF} line within experimental error. These results on the Himalayan leucogranites agree well with our data from other leucogranites from France in the Hercynian chain (closed symbols).

The next step was to identify the non-ferromagnetic minerals (called the matrix minerals) responsible for the K_{HF}. K_{HF} was measured from room temperature down to a few tens of degrees Kelvin for two Everest samples (one from the tourmaline facies and the other from the biotite facies (Fig. 4a)) and for a black tourmaline monocrystal obtained from underlying pegmatites but of the same type as encountered in the granite (Fig. 4b). A very good fit is found using Eq. (1). The D values are close to the reference values for quartz and feldspars (-14.5×10^{-6} SI; e.g., [1,3]). Therefore the lack of antiferromagnetic minerals (which should result in positive D values) is confirmed, whereas the small observed θ values are in good agreement with reference data for ferromagnesian silicates (in particular biotite, with $\theta = 20$ K, and muscovite, with $\theta \approx 0$ K [36]). Negative values for tourmaline are symptomatic of antiferromagnetic interactions. We may thus conclude that the susceptibility of these leucogranites, apart from a more or less constant diamagnetic contribution, is due to the paramagnetic silicates biotite, tourmaline, muscovite and garnet. These last two may be accessory, as garnet is a very minor constituent in these rocks, whereas muscovite, although abundant, has a very small specific susceptibility due to its low iron content. As garnet and diamagnetic silicates are practically isotropic, the AMS of these rocks is therefore mainly due to biotite or tourmaline, with probably a minor contribution from muscovite.

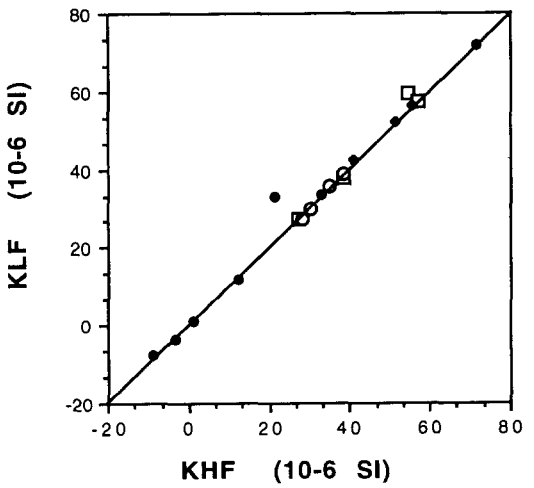

Fig. 3. Plot of low field susceptibility K_{LF} measured with the KLY-2 bridge vs. high field susceptibility K_{HF} measured with the cryogenic magnetometer (both in units of 10^{-6} SI) for 8 selected samples from Gangotri (○) and Everest (□) massifs together with 10 values from the French Hercynian leucogranitic massifs of Echassières (●) and the Pyrenees (♦).

These conclusions, which have been reached using high field measurements, may be independently tested (Fig. 2) by comparing room-temperature mean low field susceptibility K_m (measured with the KLY-2) to the weight percent of iron according to Eq. (2). In some cases manganese can make a significant contribution to paramagnetic susceptibility in granites [5]. However, geochemical analyses reveal an upper limit of 0.04% MnO_2 in our granites. If the conclusions from high field measurements are correct we can predict a correlation between K_m and the amount of Fe_2O_3 with a slope of $(46.6 + 15.1 \times R) \times (10^{-6}$ SI per total Fe_2O_3%). The oxidation ratio, $R = t''/(t + t')$, can vary from 0 to 1 and therefore the slope must be between 46.6 and $61.6 \times (10^{-6}$ SI per total Fe_2O_3%). In Fig. 2, K_m corrected from quartz diamagnetism shows a linear correlation with weight percent iron, the best fit being found for Everest massif, which displays a larger range of amount of iron. In that massif, error bars corresponding to the dispersion between specimens from the same block are shown. Most data fall within the expected limits (dashed lines). R values derived from slopes forced through the origin are 0.31, 0.47 and 0.52 respectively for the Everest, Gangotri and Manaslu datasets. The mean derived from susceptibility measurements compares favourably with that obtained from 5 wet chemical analyses of the Gangotri massif ($R = 0.54 \pm 0.04$ [10].

5.2. Ferromagnetic grains and the origin of NRM

NRM was measured in all samples using a cryogenic magnetometer (noise level of < 0.01

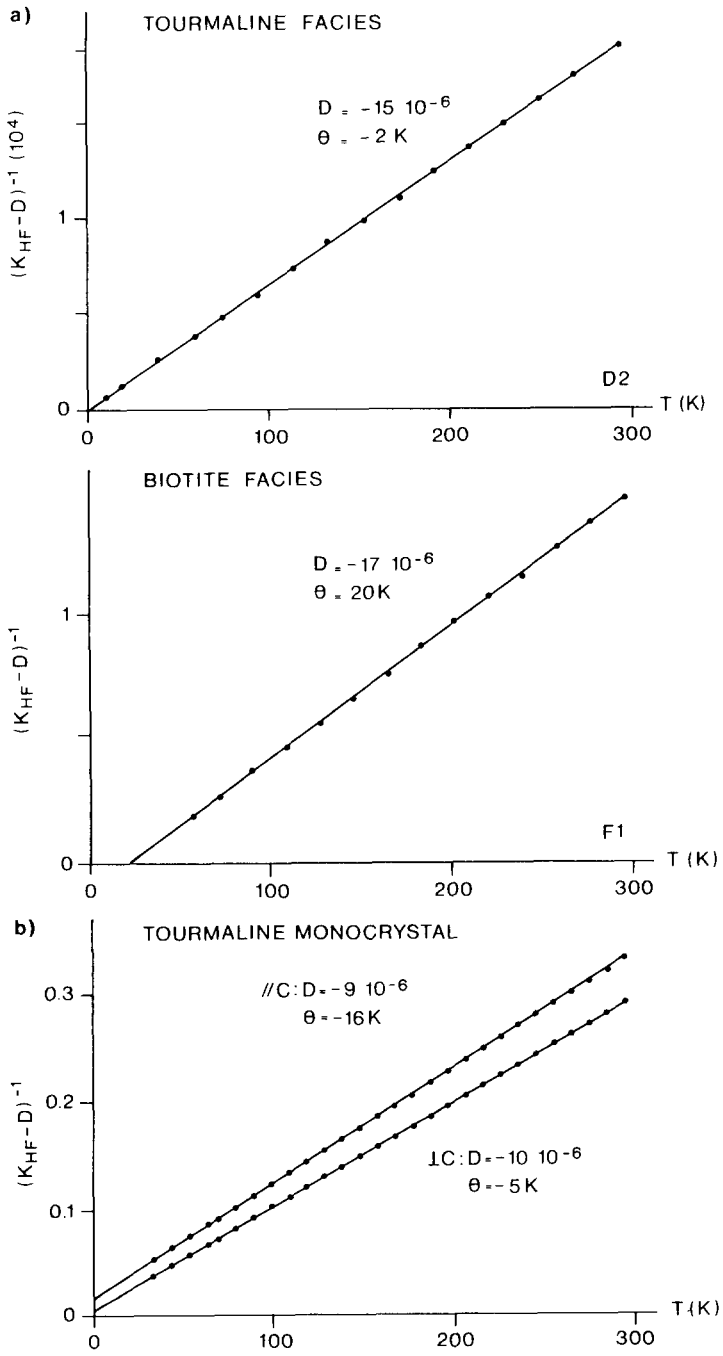

Fig. 4. Inverse of the high field susceptibility K_{HF} (measured in 3 T, and in 10^4 SI) corrected from the diamagnetic contribution D vs. absolute temperature. The D value is adjusted to obtain the best linear fit. (a) For 2 samples from the Everest leucogranite. (b) From a tourmaline monocrystal with measurement done either parallel or perpendicular to the c-axis.

mA/m), although for the Manaslu samples only a Molspin spinner (noise level of 0.05 mA/m) was available. The samples were exceptionally weak and often not measurable. All the samples have intensities of less than 0.1 mA/m, with the exception of one block from Manaslu (values close to 0.1) and 4 blocks from 3 outcrops in Everest (blocks C1, D1, D2 and E2), where intensities can reach a few mA/m. Such low values accord with the negligible ferromagnetic contribution in K_{LF} and the very low values of saturation IRM. IRM varies from 10 to 30 mA/m in the samples whose NRM is < 0.1 mA/m. Such a low level of ferromagnetic trace (an IRM of 10 mA/m corresponds to about 1 ppm of fine-grained magnetite and about 20 ppm of hematite) is equivalent to that encountered in very pure platform limestones [37]. Paleomagnetic investigation has therefore been completed only at site C, D and E in the Everest massif. Contrasting behaviour appears during AF demagnetization: The NRM of site D is practically fully demagnetized in 100 mT with a median destructive field of 28 mT (Fig. 5), whereas AF treatment has only a marginal effect in site C and E. Accordingly, progressive acquisition of IRM reveals increasingly coercive minerals at site D, E and C, with half-acquisition fields of 15, 50 and 130 mT respectively. Stepwise thermal demagnetization applied after the AF (Fig. 5), together with continuous measurement of NRM during heating (Fig. 6), shows single-component behaviour at sites D and E with narrow unblocking just below Curie temperatures at 500 and 340°C respectively. The NRM at site C is still strong above 600°C, although reaching a stable end point appeared impossible. At site E a small component persists above 350°C in samples not previously subjected to AF, pointing towards a minor contribution of the same type as at site D. Based on these results we can identify the ferromagnetic minerals present as titanomagnetite at site D, pyrrhotite with minor (titano)magnetite at

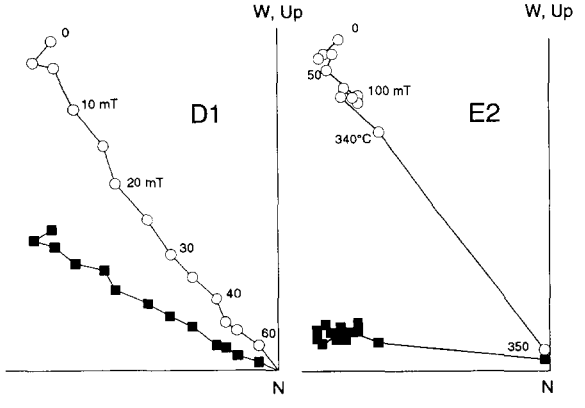

Fig. 5. Orthogonal projections (Zijderveld plots) of the NRM vector during AF demagnetization. In sample E2 we also show the subsequent thermal demagnetization.

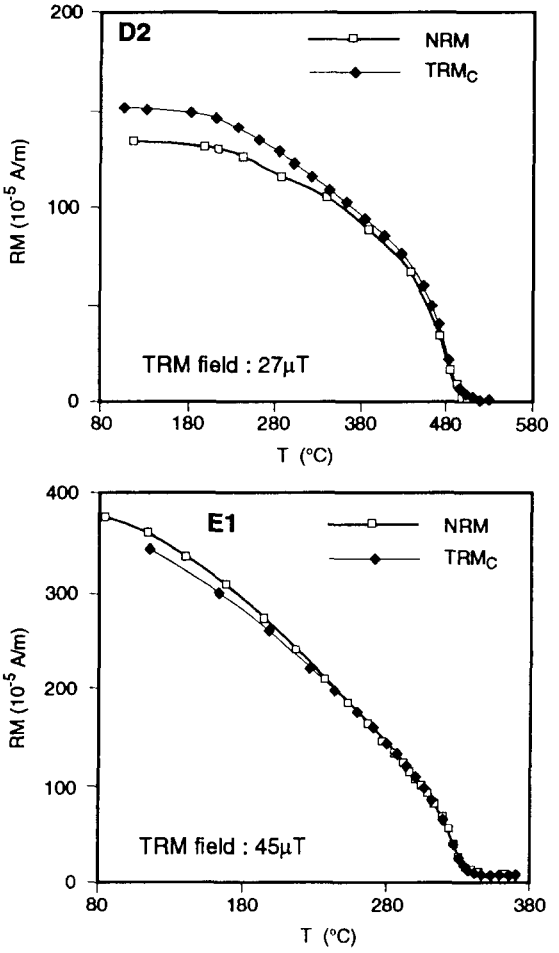

Fig. 6. Intensities of NRM and TRM_c (in 10^{-5} A/m) during heating in zero field and in a nitrogen atmosphere at a rate of 2°/min. TRM was acquired directly after NRM demagnetization using $H_{lab} = 45$ μT. Measured TRM was adjusted to NRM near the Curie point using the law $TRM_c = TRM \times H_{pal} / H_{lab} + \text{constant}$.

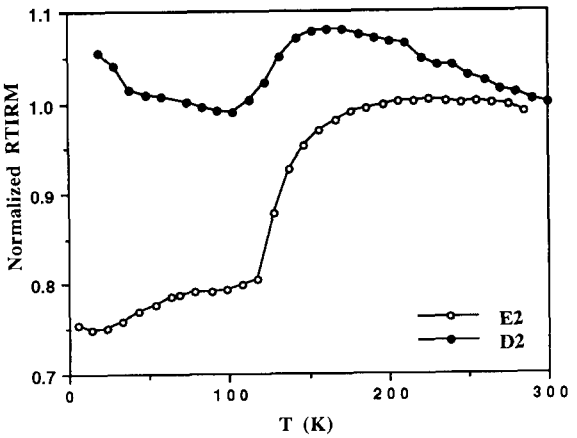

Fig. 7. Cooling curves of IRM acquired at room temperature in 3 T for samples E2 and D2.

site E and hematite at site C. The composition of the titanomagnetite deduced from the observed maximum blocking temperature, which is assumed to be equal to the Curie point, is $Fe_2(Fe_{0.8}Ti_{0.2})O_4$. The low-temperature behaviour of the IRM has been measured on samples D2 and E2 (Fig. 7) to further characterize their magnetic mineralogy [32,37]. Whereas a clear Verwey transition above 120 K definitely identifies pure magnetite as the soft component in sample E2, only a faint change in slope of the IRM curve occurs near 30–40 K. The identification of pyrrhotite by this method appears, therefore, quite unsuccessful. In sample D2 the room-temperature IRM shows a steady increase with decreasing temperature (symptomatic of titanomagnetite) but also a small Verwey transition pointing toward some pure magnetite in the sample.

Such a variety of magnetic minerals which have different stability fields is surprising within the same pluton, and we may also note that significant ferromagnetic contributions are only found in the 3 tourmaline-bearing sites. Pyrrhotite and hematite (both observed in only one block from the same site, the hematite-bearing rock being orange coloured) are likely to be secondary products of hydrothermal or epigenic alteration rather than minerals crystallized primarily in the magma.

From a petrological point of view, the presence of very small amounts of hematite and the magnetite points to quite oxidizing conditions. This contrasts with the inferred strongly reduced character of these granites, which are likely to have been derived from the partial melting of a graphite-bearing pelitic source where the oxygen fugacity (fO_2) should have been very low. Indeed, experiments carried out on a Manaslu sample have shown that, under moderately reducing conditions around the Ni–NiO buffer curve, magnetite is an important accessory phase, in contrast with the current paragenesis of the leucogranite which is optically almost free of opaques [38]. On the other hand, under more reducing conditions, at or below the fO_2 defined by the QFM buffer curve, this mineralogical requirement is fulfilled (i.e., no opaques are present [26]). These results imply that the occurrence of these opaque minerals (hematite, magnetite and pyrrhotite) must be ascribed to late oxidation processes. Their low abundance suggests that this occurred when almost all the iron was already locked in the ferromagnesian silicates, i.e. when the system was closed or below its solidus.

The curves of continuous thermal demagnetization presented for D2 and E1 (Fig. 6) are quite similar for TRM and NRM, apart from the fact that the TRM of E1 shows a residue with linear decrease above the Curie point of 340°C due to the minor magnetite contribution. TRM curves have been fit to the NRM curves in the temperature range just below the Curie point by multiplying the TRM by a correcting factor h and removing the linear trend in the TRM above 340°C for E2. Factor h gives us an estimated apparent paleointensity if we assume that NRM is a TRM acquired during cooling of the granite in the geomagnetic field. This paleointensity, $H_{pal} = h \times H_{lab}$, appears to be, respectively, 45 and 27 μT for E1 and D2. These values accord with the value of 37 μT for the latitude of Everest (28°N) calculated according to the mean dipole moment for the last 5 Ma [39]. This experiment thus strongly suggests that the NRM at site D and E is a TRM acquired during cooling of the pluton below, respectively, 500 and 340°C in a stable geomagnetic field. This 'paleointensity test' con-

Table 1
Averaged characteristic paleomagnetic directions (N = site number for western Nepal data, and specimen number for the Everest sites)

Site	N	D	I	K	α_{95}
D	16	204.5	−49.7	285	2.2
D corrected with AAS	–	202	−47.5	–	–
E (pyr.)	8	186.1	−52.5	250	3.5
E (magn.)	7	207.9	−58.3	16	15.5
Western Nepal [40]	12	196.4	−65.9	183	3.2

stitutes another argument for assigning a formation temperature to the different magnetic minerals: above 500°C for the probably primary titanomagnetite of site D, above 340°C for the possibly hydrothermal pyrrhotite, and below 600°C for the hematite of site C with a probable epigenic origin.

6. Preliminary interpretation of paleomagnetic directions

Characteristic directions were obtained from the 4 different blocks using various procedures:

(i) Specimens from blocks D1 and D2 where demagnetized by AF in 20 mT, as pilot AF demagnetization revealed single-component behaviour (Fig. 5). Continuous thermal demagnetization too showed no change in directions up to the Curie point. Very good consistency in the directions is found within each block and for both blocks, as shown by the Fisherian statistics (Table 1).

(ii) Block E2 was heated in 30°C steps up to 370°C; no significant change in directions was observed but a sudden drop in intensity occurred between the last two steps. A direction characteristic of the TRM carried by pyrrhotite (A) was computed from the vector difference between these two steps whereas a 'magnetite' component (B) was derived from the residual NRM directions.

(iii) Samples of block C1 were heated stepwise up to 650°C but the directions became unstable. During continuous heating the direction of a given sample remained constant up to the Curie point; however, the different samples yield quite dispersed directions, with shallow negative inclination and declination varying from 200 to 300°. Due to this inconsistency within the same block, no characteristic direction was computed here.

The characteristic directions appear to have an inclination that is steeper than the expected value of 42° (computed at 15 Ma for the Indian plate assuming a northward drift of 2 cm/a [7]), and a declination corresponding to an apparent clockwise rotation of $25 \pm 2.5°$ for site D and $6 \pm 3.5°$ for site E (assuming negligible rotation of India since 15 Ma).

Assuming an age of NRM acquisition of 15 Ma (very rapid cooling of such granites is inferred, in particular from the low temperature of the country rock and rapid uplift), the inclination difference is 8 and 10° respectively for site D and E. Despite the small number of samples these values have real significance, due to the very small α_{95} and the good control on the movement of India. Moreover, these steep inclinations have also been observed in a well-documented study of limestones from west Nepal ([40]; see also [41]) that were remagnetized during late Tertiary metamorphism. Following [40] we interpret our preliminary results as being due to tilting of the order of 10° of the entire region toward the north. The large area affected by such tilting requires a deep-seated process, the best candidate being either the presence of a ramp on the MCT which would have been climbed by the Tibetan slab after the time of acquisiton of NRM [15] or the activation of the MBT. The present-day tilt rate of 3.4°/Ma observed in the Lesser Himalayas over a 50 km wavelength shows the likelihood of such a hypothesis [42].

To account for the declination difference between our data and true northe, it is again possible to find a local explanation in terms of a gentle late folding around a N–S axis of the Everest intrusion, or a more regional one, following the oroclinal bending model of [41]. Due to their limited extent, however, the present data are barely significant in terms of rotation around a vertical axis.

7. Anisotropy of magnetic susceptibility

7.1. Directional results

We will report here only briefly the data on Gangotri and Manaslu as they are the subject of separate publications on structural interpretation [10,11]. It is clear that the three massifs share the same type of magnetic behaviour. At Everest (Fig. 8a), all sites but one (site E) reveal quite well grouped K_1 and K_3 directions. At Gangotri

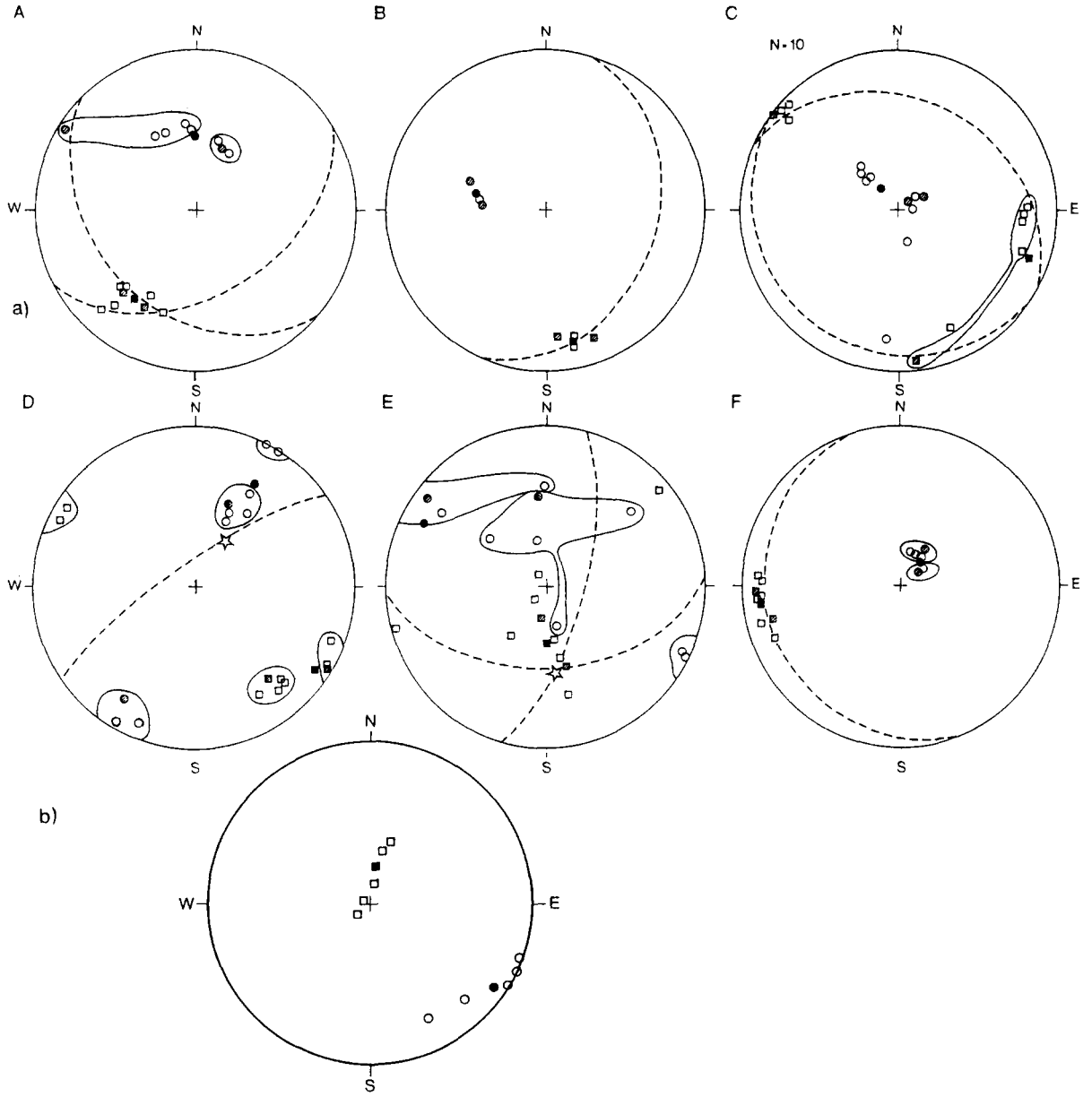

Fig. 8. (a) Six stereoplots showing, in geographic coordinates, the directions of maximum (squares) and minimum (circles) susceptibilities K_1 and K_3 for the 6 sites on the Everest massif. Structural foliation (dashed line) and lineation (star), determined on each block whenever possible, is indicated. Data for large-volume sample appear as shaded symbols, and average directions as black symbols. At some sites with two blocks all directions from the same block are enclosed with a solid line. Number of specimen at a site and average L and F values are indicated. (b) AAS results for site D.

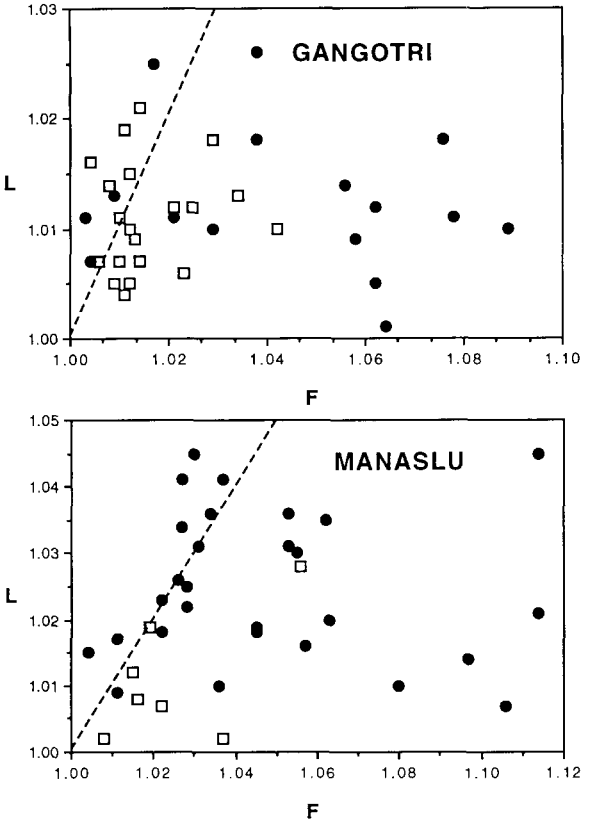

Fig. 9. Plot of site-average anisotropy ratio L vs. F (mean block values) for the Gangotri and Manaslu massifs with tourmaline and biotite indicated separately (□ and • respectively).

and Manaslu, directions appear dispersed at only 8 and 4 sites respectively. Reasons for such dispersion may be the following:

(1) Measurement uncertainty due to the KLY-2: However, the L and F values are much larger than the sensitivity limit (Fig. 9 and Table 2), and at all sites the confidence angles on individual directions are always less than 10°.

(2) Heterogeneity of the fabric at the specimen scale due to the large grain size of some facies in the granite: In fact, the preferred orientation of only a few tens of ferromagnesian grains may be averaged when measuring a 10.8 cm^3 sample. The presence of such a grain size effect should be detectable in the Everest dataset where 65 and 10.8 cm^3 samples were cut from the same block, and indeed this effect is visible at site E where the directions for the large sample appear in the centre of the group defined by the small-sample data. In the other Everest blocks the large-sample directions do not appear less dispersed, whereas on the other hand within-site heterogeneity is exemplified by the significant difference in mean directions between two blocks from the same site (site A, D, E and F in Fig. 8a).

(3) Presence of two minerals that contribute to the AMS in variable amounts and with various orientations resulting in a dispersion of the total anisotropy: This is suggested by the fact that dispersed directions are only found at sites in mixed (tourmaline and biotite) facies (Fig. 8a, site E).

7.2. Correlation between magnetic anisotropy and petrofabric

This last possibility, which probably explains the main part of the dispersion, is strongly sup-

Table 2
AMS and AAS* mean results for the Everest sites, with facies (b = biotite, t = tourmaline, m = mixed) indicated in parentheses. K_m (with standard deviation) is in 10^{-6} SI. For K_1 and K_3 we give the tensorial averaged declination and inclination with the two half angles of the confidence ellipse [27] in parentheses.

Site	N	K_m	L	F	K_1	K_3
A (b)	8	37.8 (2.5)	1.019	1.025	215.32 (7.4)	359.52 (18.3)
B (b)	4	44.8 (6.7)	1.010	1.077	168.17 (19.9)	282.54 (18.1)
C (b)	10	52 (161)	1.008	1.034	110.12 (37.15)	321.76 (18.8)
D (t)	10	12.6 (14.9)	1.021	1.018	125.9 (12.3)	30.26 (28.4)
D* (t)	5	–	1.20	1.25	11.72 (33.3)	125.8 (35.4)
E (m)	10	12.3 (14.6)	1.018	1.003	179.61 (23.4)	298.15 (49.12)
F (b)	8	50.2 (4.8)	1.014	1.063	263.12 (9.2)	41.74 (5.2)

ported when considering the correlation between magnetic and structural directions at sites with only one type of dark mineral. At biotite-bearing sites (A, B, C and F) K_3 directions, instead of K_1 for tourmaline-bearing sites (D), appear well grouped at the pole of the observed foliation (Fig. 8a). Structural lineation is only visible at sites D and E in the tourmaline-bearing facies, due to the fact that tourmaline grains occur as elongate rods, which are much more sensitive to linear preferred orientation than platelets of biotite or muscovite. At site D (and at the tourmaline-bearing sites of Gangotri and Manaslu) K_3 appears parallel to the mineral lineation (i.e., the reverse of that which would be expected for anisotropy due to phyllosilicate). This 'inverse' characteristic of tourmaline is also confirmed by the fact that at mixed facies site E one sample (probably richer in tourmaline) has K_3 parallel to the lineation, whereas the others have K_1 along that direction.

What is the physical explanation for such an unusual relationship between structural and magnetic directions? It is well known [1] that phyllosilicates, with K_3 perpendicular to the basal plane of the crystal and $K_1 = K_2$, result in a 'normal' fabric, whereas occurrences of inverse fabric have been recently reported as being due to single-domain magnetite [43,44] or to paramagnetic carbonates [43,45,46]. In the present case, however, the AMS must be due to the tourmaline crystals. Indeed, low field measurements on several tourmaline monocrystals from Nepal and India yield a K_3 parallel to the c-axis of the rhombohedral structure (i.e., elongated crystals). K_1 appears equal to K_2 (i.e., $L = 1$), in accordance with the crystalline symmetry of revolution. One black tourmaline monocrystal (of the same type as that occurring in the leucogranites) has also been measured along and perpendicular to the c-axis, at high field and variable temperature (Fig. 4c). The resulting curves clearly demonstrate that the susceptibility and anisotropy observed in those grains is the intrinsic paramagnetic behaviour and not the result of oriented ferromagnetic inclusions.

This peculiar magnetic behaviour clearly explains why, in rocks whose AMS is due to tourmaline (e.g., site D), K_3 is parallel to the structural lineation and K_1 is parallel to the pole of

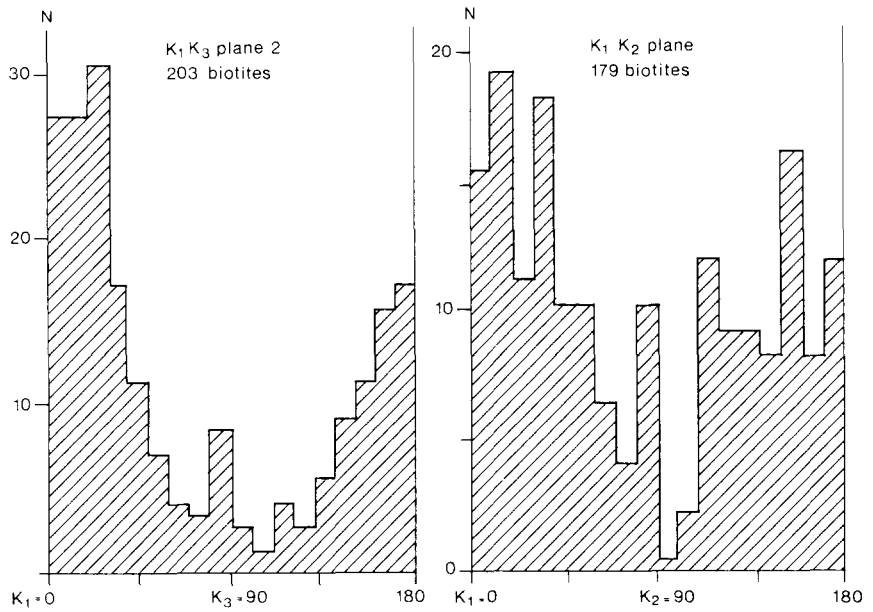

Fig. 10. Histograms of biotite plane orientations in two perpendicular thin sections from Everest site F cut within the planes K_1–K_3 and K_1–K_2.

structural foliation. Conversely, the significance of L and F must be inverted with respect to, for example, biotite-bearing rocks: a strongly planar preferred orientation should result in $L \gg F$. To further characterize the fabric at tourmaline site D, AAS measurements (Fig. 8b) can be compared to AMS measurements. For the ferrimagnetic grains fabric revealed by AAS K_1 now appears parallel to the structural lineation and K_3 to the pole of foliation. Somewhat higher anisotropy ratio are found for AAS (Table 2), leading us to suspect a significant deflection in the NRM from the acquisition field direction. However, the corrected paleomagnetic direction for site D, computed using the technique of [47] and assuming that the anhysteretic and thermoremanent tensors are proportionnal, is only slightly different from the uncorrected data, thus confirming the interpretation in section 6.

In the measured black tourmalines the K_m and F values are quite constant, at 950×10^{-6} SI and 1.12 respectively. This F value can be compared to the much higher values found in biotite (around 1.35 [36,48]) and muscovite (around 1.2 [36,49]). This difference can be detected in the anisotropy ratio measured in our leucogranites (Fig. 9). Site mean values for biotite-bearing sites are, on average, larger than the values for tourmaline-bearing sites, with a much stronger tendency toward planar ($F \gg L$) fabrics. As a result of the inversion of the tourmaline magnetic fabric we would expect symmetric behaviour of the tourmaline-bearing sites ($L \gg F$). However, they actually appear with a more neutral shape ($L \approx F$) due to the fact that linear markers, such as the tourmaline rods, record the flattening deformation (which appears dominant in these granites) less easily than planar markers.

To check our contention that AMS represents a precise measurement of the biotite petrofabric in the biotite-facies samples we used the image analyser system to measure preferred orientations of biotite planes in two perpendicular thin sections from site F cut within the K_1–K_3 and K_1–K_2 planes (Fig. 10). In the first plane the strong foliation of biotite appears strictly parallel to K_1. Within the magnetic foliation plane biotite is weakly oriented (in accordance with the lack of visible lineation) but a faint maximum appears parallel to K_1. This is consistent with the suggestion that K_1 actually measures the stretching lineation of the granite with much better accuracy than traditional petrofabric measurements, as is visible on the stereoplot for site F (Fig. 8a).

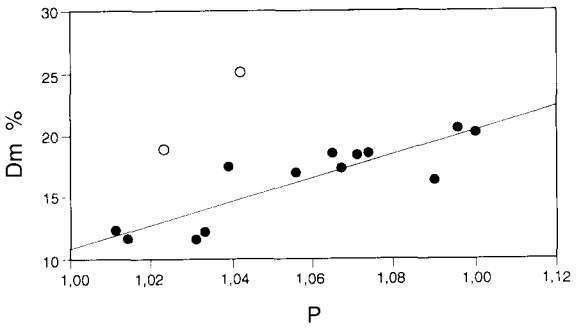

Fig. 11. Intensity of biotite petrofabric D_m [34,10] vs. degree of magnetic anisotropy P determined from thin section observations for 15 samples of the Gangotri massif.

In principle it is also possible to make semi-quantitative use of anisotropy ratio L and F to characterize the intensity of the fabric. However, due to the possible contamination by tourmaline and the variation in the relative contribution of muscovite this application, even restricted to the same lithological facies, remains difficult. Nevertheless a rather good correlation has been found in 19 samples of the biotite-bearing facies in the Gangotri granite between the degree of magnetic anisotropy P and the intensity of preferred orientation of biotite determined by image analysis (Fig. 11, after [10]). Anomalously low P values found in two samples (circles) correlate well with a minor occurrence of tourmaline in these samples.

The primary nature of the paramagnetic minerals is well established for muscovite and biotite in these granites [10,26], although there is in some cases evidence that tourmaline formed later in the crystallization in relation with boron-bearing mineralized pegmatitic fluids. However, when tourmaline appears disseminated regularly throughout the outcrop with consistent preferred orientation, its early formation in the magma is most likely. The observed lineations, which correspond to the preferred orientation of the long

axes of ferromagnesian grains formed early during crystallization of the magma, definitely reflect the high-temperature deformation of the magmatic body when it was still viscous. Indeed, apart from localized shear zones no trace of solid-state deformation has been observed in these granites. We therefore have access to either the flow line in the magma during its emplacement or to the subsequent stretching direction of the viscous granitic body included in a deforming crustal section. Whereas the first case is exemplified in granites emplaced in relatively stable area, with subvertical or divergent lineations, the second case, with consistent subhorizontal lineation over a large area, is probably the rule in syntectonic granites [6].

7.3. Structural interpretation

The main structural application of these AMS measurements is therefore in the mapping of lineations that are characteristic of the emplacement kinematics that would not have been accessible by other means. Due to the magnetic mineralogy the lineation corresponds either to K_1, for the biotite facies, or to K_3, for the tourmaline facies. To decide between the two options, visual examination of the mineral assemblage may be implemented by comparison of the structural foliation, which is usually faintly visible on the samples, with either K_3 (the normal case) or K_1 (the inverse case). This method may leave some ambiguity however, especially in mixed facies and at some tourmaline-bearing sites where muscovite is also common, and may therefore result in a normal fabric dominating the inverse fabric of the tourmaline.

To estimate the relative importance of muscovite we must consider specifically K_m, which is more or less proportional to the amount of iron (of the order of $1–1.8 \times 10^{-3}$ SI for biotite and 5×10^{-5} SI for muscovite [3,36,48,49]). Garnet, which has been mentioned as an accessory paramagnetic mineral in these rocks, cannot contribute to the anisotropy due to its cubic system (measurements on garnet gems from Nepal actually show $P \leq 1.002$ and $K_m \approx 3.2 \times 10^{-3}$ SI. Modal analysis of thin sections from the Gangotri massif reveals that as the geochemical fractionation proceeds (i.e., as tourmaline abundance increases) the proportion of muscovite decreases down to 4–5%, whereas the tourmaline contribution, which is albeit difficult to estimate accurately owing to the large size of the tourmalines at the thin section scale, is around 5–7% [25]. In this case, less than 10% of the susceptibility will be due to muscovite, and therefore tourmaline should be largely predominant and the role of muscovite should only be to lower the anisotropy ratio (thus reinforcing the tendency in Fig. 9).

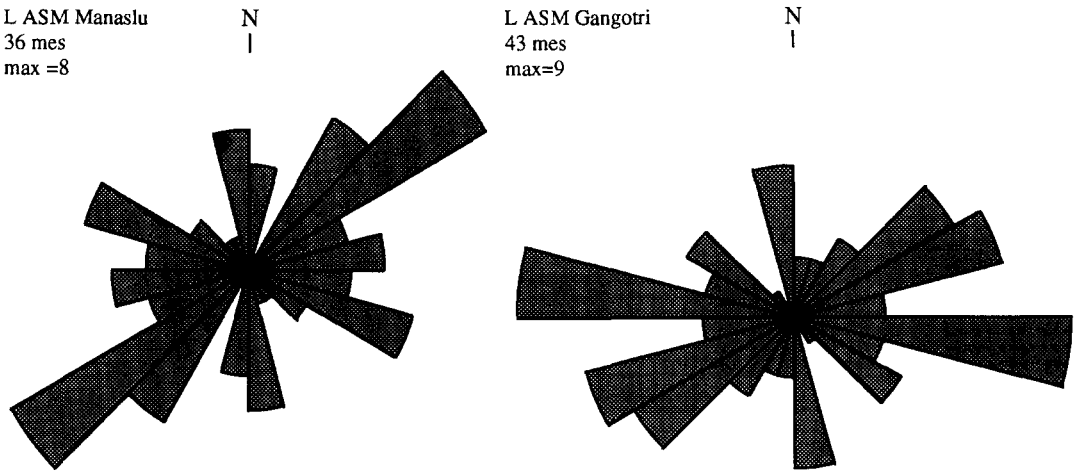

Fig. 12. Rose diagram of stretching lineation azimuths derived from AMS mean site data in Gangotri and Manaslu.

Is there a magnetic method to decide which of these three anisotropic paramagnetic minerals is chiefly responsible for the AMS directions? In principle we could use the θ values determined in Fig. 4. This method, based on contrasting θ values in the three minerals, is described at length in [3]. In our situation, apart from the difficulties of the experiment this method will be conclusive mainly in the non-mixed facies. Therefore, from a conservative standpoint, it is not possible to take into account anisotropy data from mixed facies when not correlated with structural measurements (see the case of site E in Fig. 8a).

Once the mineralogical interpretation has been carried out, lineation and foliation maps can be derived from the AMS data. The foliations usually appear to be gently dipping. A magnetic lineation map has been derived and is compared to the map of lineations measured in the field for Gangotri [10] and Manaslu [11]. The three sets of data compare favourably and are characterized by a rather dispersed pattern (rose diagrams in Fig. 12 for Gangotri and Manaslu; Fig. 1b for Everest). In the Gangotri massif, however, a roughly E–W dominant trend appears, and this has been interpreted as resulting from the effect of the late movements of the dextral wrench zone operating at the top of the Tibetan slab [10]. In the Manaslu massif a more NE–SW trend is apparent. This last direction is oblique to the E–W strike of the dextral shear zone, which was also active in this area at the time of granite emplacement [11,23]. Thus it is possible that, in the Manaslu pluton and in contrast to the Gangotri, part of the fabric represents remnants of a N–S stretching lineation associated with the extension [17,18], this fabric having been later reoriented by the dextral shear movement. In the Everest massif, the presence of both the N–S and E–W stretching directions suggests that such a phenomenon may also have occurred in this area, although the small number of data collected preclude any conclusive statement. We may note, however, that E–W lineations are concentrated in the eastern part where the pluton is thicker [50] and where slightly higher levels in the granite have been sampled.

8. Conclusions

The High Himalayan leucogranitic belt has been examined in three different places and reveals quite homogeneous behaviour in terms of magnetic properties. Low field magnetic susceptibility, K_m, is less than 10^{-4} SI and is entirely of diamagnetic and paramagnetic origin. This can be demonstrated using high field susceptibility measurements and by correlating K_m with iron content. The paramagnetic minerals responsible for the anisotropy of magnetic susceptibility are biotite (with a minor contribution from muscovite) and tourmaline, which leads, respectively, to a normal and reverse magnetic fabric (i.e., with either K_3 or K_1 parallel to the pole of structural foliation).

AMS is very efficient at detecting the high-temperature fabric of these granites because of magmatic flow and deformation in the viscous state, which helps in understanding the condition of emplacement of these syntectonic plutons.

The directions of the stretching lineation revealed by the use of the AMS method display a rather dispersed pattern, a result which is somewhat surprising with respect to the tectonic framework of the High Himalayan leucogranites. Further, this tectonic pattern is not similar in the different massifs surveyed. The Gangotri massif has an E–W dominated structure which is accounted for by the effect of a dextral shear zone active at the top of the Tibetan slab. On the other hand, the Manaslu and Everest massifs share E–W, N–S or intermediate stretching directions, which may indicate that these granites have recorded part of the N–S kinematic movements associated either with the thrusting on the MCT or with the subsequent N–S extension; part of this movement may have been associated with the dextral wrench movement. To a first approximation this would indicate that the timing of intrusion of these massifs relative to the movement on the MCT and to the dextral wrench faulting may have changed across the entire range. Thus the Gangotri massif would have been emplaced later, mainly bearing a trace of the Miocene dextral shear zone, whereas the Manaslu and Everest

massifs would have been intruded earlier, thus recording both the late movement of the MCT and that related to the dextral shear zone. Alternatively, it cannot be ruled out that these tectonic phases were not synchronous.

NRM is significant only at two sites on the Everest massif, where it yields very well defined reversed directions. It appears to correspond to a TRM carried by either titanomagnetite or pyrrhotite, which have recorded the recent movements of the pluton after its cooling below 300°C. The discrepancy with the predicted Indian direction suggests northward tilting of the area, in accordance with other paleomagnetic data from Nepal, and possible slight clockwise rotation. However, a larger sampling would be necessary to place these preliminary interpretations on firmer ground and to enable the discarding of possible incomplete averaging of the secular variation.

Acknowledgements

Field work for this study was supported by various grants from the INSU–CNRS. We thank D. Kent, D Schneider, R. Dunn, M. Fuller, M. Jackson and S. Banerjee for their help in the paleomagnetic measurements at the LDGO in New York, at the University of Santa Barbara and at Minneapolis. B.B. Ellwood, C. Klootwijk and the anonymous reviewers are thanked for their help in improving the manuscript. [*PT*]

References

[1] F. Hrouda, Magnetic anisotropy of rocks and its application in geology and geophysics, Geophys. Surv. 5, 37–82, 1982.

[2] G.J. Borradaile, Magnetic susceptibility, petrofabric and strain—a review, Tectonophysics 156, 1–20, 1988.

[3] P. Rochette, M. Jackson and C. Aubourg, Rock magnetism and the interpretation of the anisotropy of magnetic susceptibility, Rev. Geophys. 30, 209–226, 1992.

[4] B.B. Ellwood, Flow and emplacement directions determined for selected magmatic bodies using anisotropy of magnetic susceptibility measurements, Earth Planet. Sci. Lett. 41, 254–264, 1978.

[5] S. Bernier, J.L. Bouchez and P. Rochette, Anisotropie de la susceptibilité magnétique du granite de Beauvoir (sondage GPF d'Echassières, Massif Central français), C.R. Acad. Sci. Paris 305, 1167–1173, 1987 (note présentée par X. Le Pichon).

[6] J.L. Bouchez, G. Gleizes, T. Djouadi and P. Rochette, Microstructure and magnetic susceptibility applied to emplacement kinematics of granites: the example of the Foix pluton (French Pyrenees), Tectonophysics 184, 157–171, 1990.

[7] J. Besse and V. Courtillot, Paleogeographic maps of the Indian Ocean bordering continents since the Early Jurassic, J. Geophys. Res. 93, 11791–11808, 1988.

[8] C.T. Klootwijk, A review of Indian Phanerozoic paleomagnetism: implications for the India–Asia collision, Tectonophysics 105, 331–353, 1984.

[9] C.T. Klootwijk, J.S. Gee, J.W. Pierce, G.M. Smith and P.L. McFadden, An early India–Asia contact: paleomagnetic constraints from Ninty East ridge, ODP Leg 121, Geology 20, 395–398, 1992.

[10] B. Scaillet, A. Pecher, P. Rochette and M. Campenois, The Gangotri Granite (Garwhal Himalaya): laccolithic emplacement in an extending collisional belt, J. Geophys. Res. 99, in press, 1994.

[11] S. Guillot, A. Pecher, P. Rochette and P. Le Fort, The emplacement of the Manaslu granite: field and magnetic susceptibility constraints, in: Himalayan Tectonics, Geol. Soc. London Spec. Publ. 74, 413–428, 1993.

[12] P. Le Fort, M. Cuney, C. Deniel, C. France-Lanord, S.M. Sheppard, B.N. Upreti and P. Vidal, Crustal generation of the Himalayan leucogranites, Tectonophysics 134, 39–57, 1987.

[13] J.L. Bouchez and A. PÊcher, The Himalayan Main Central Thrust pile and its quartz-rich tectonites in Central Nepal, Tectonophysics 78, 23–50, 1981.

[14] M. Brunel, Ductile thrusting in the Himalayas: shear sense criteria and stretching lineation, Tectonics 5, 247–265, 1986.

[15] J.P. Burg, M. Brunel, D. Gapais, G.M. Chen and G.H. Liu, Deformation of leucogranites of the crystalline Main Central Sheet in southern Tibet, J. Struct. Geol. 6, 535–542, 1984.

[16] E. Herren, Zanskar shear zone: northeast–southwest extension within the Higher Himalaya, Geology 15, 409–413, 1987.

[17] M. Mattauer and M. Brunel, La faille normale Nord-Himalayenne (FNNH): conséquence probable d'un diapirisme granitique, C.R. Acad. Sci. Paris 308, 1285–1289, 1989.

[18] B.C. Burchfiel and L.H. Royden, North–south extension within the convergent Himalayan region, Geology 13, 679–682, 1985.

[19] R. Caby, A. PÊcher and P. Le Fort, Le grand chevauchement central himalayen: nouvelles données sur le métamorphisme inverse à la base de la dalle du Tibet, Rev. Géol. Dyn. Géogr. Phys. 24, 89–100, 1983.

[20] A. PÊcher and B. Scaillet, La structure du Haut Himalaya au Garwhal (Indes), Eclogae Geol. Helv. 82, 655–668, 1989.

[21] P. Molnar and P. Tapponnier, Active tectonics of Tibet, J. Geophys. Res. 8, 5361–5375, 1978.
[22] P. Tapponnier, G. Peltzer and R. Armijo, On the mechanics of the collision between India and Asia, in: Collision Tectonics, M.P. Coward and A.C. Riess, eds., Geol. Soc. London Spec. Publ. 19, 115–157, 1986.
[23] A. PÊcher, J.L. Bouchez and P. Le Fort, Miocene dextral shearing between Himalaya and Tibet, Geology 19, 683–685, 1991.
[24] R. Armijo, P. Tapponnier and T. Han, Late Cenozoic right-lateral strike-slip faulting in southern Tibet, J. Geophys. Res. 42, 11236–11268, 1989.
[25] B. Scaillet, C. France-Lanord and P. Le Fort, Badrinath–Gangotri plutons (Garhwal, India): petrological and geochemical evidence for fractionation processes in a high Himalayan leucogranite, J. Volcanol. Geotherm. Res. 44, 163–188, 1990.
[26] B. Scaillet, M. Pichavant and J. Roux, Tourmaline, biotite and muscovite stability in felsic peraluminous liquids, EOS Trans. 72, 311, 1991.
[27] V. Jelinek, Statistical processing of anisotropy of magnetic susceptibility measured on a group of specimens, Stud. Geophys. Geodet. 22, 50–62, 1978.
[28] M. Jackson, Anisotropy of magnetic remanence: a brief review of mineralogical sources, physical origins and geological applications, Pure Appl. Geophys. 136, 1–28, 1991.
[29] C. McCabe, M. Jackson and B.B. Ellwood, Magnetic anisotropy of the Trenton limestone: results of a new technique, anisotropy of anhysteretic susceptibility, Geophys. Res. Lett. 12, 333–336, 1985.
[30] P. Rochette, G. Ménard and R. Dunn, Thermochronometry and cooling rates deduced from single sample records of successive magnetic polarity events in uplifting metamorphic rocks, Geophys. J. Int. 108, 491–501, 1992.
[31] P. Rochette, G. Fillion, P. Mollard and R. Vergne, Utilisation d'un magnétomètre à effet Josephson pour l'analyse de l'anisotropie magnétique des roches, C.R. Acad. Sci. Paris 296, 557–558, 1983.
[32] P. Rochette, G. Fillion, J.L. Mattéi and M. Dekkers, Magnetic transition at 30–34 K in Fe_7S_8: insight into a widespread occurrence of pyrrhotite in rocks, Earth Planet. Sci. Lett. 98, 319–328, 1990.
[33] P. Rochette, Magnetic susceptibility of the rock matrix related to magnetic fabric studies, J. Struct. Geol. 9, 1015–1020, 1987.
[34] F. Lapique, M. Champenois and A. Cheilletz, Un analyseur vidéographique interactif: description et applications, Bull. Minéral. 111, 679–687, 1988.
[35] O. Jover, P. Rochette, J.P. Lorand, M. Maeder and J.L. Bouchez, Magnetic mineralogy of some granites from the French Massif Central: origin of their low field susceptibility, Phys. Earth Planet. Inter. 55, 79–92, 1989.
[36] O. Ballet, Fe^{2+} dans les silicates lamellaires: étude magnétique et Mössbauer, Thesis, Univ. Grenoble, 1979.
[37] W. Lowrie and F. Heller, Magnetic properties of marine limestones, Rev. Geophys. Space Phys. 20, 171–192, 1982.
[38] F. Benard, P. Moutou and M. Pichavant, Phase relations of tourmaline leucogranites and the significance of tourmaline in silicic magma, J. Geol. 93, 271–279, 1985.
[39] M. Prévot, M. Derder, M. McWilliams and J. Thompson, Intensity of the Earth magnetic field: evidence for a Mesozoic dipole low, Earth Planet. Sci. Lett. 97, 129–139, 1990.
[40] E. Appel, R. Muller and R.W. Widder, Paleomagnetic results from the Tibetan sedimentary series of the Manang area, Geophys. J. Int. 104, 255–266, 1991.
[41] C.T. Klootwijk, P.J. Conaghan and C. Powell, The Himalayan arc: large-scale continental subduction, oroclinal bending and back-arc spreading, Earth Planet. Sci. Lett. 75, 167–183, 1985.
[42] M. Jackson, S. Barrientos and R. Bilham, Uplift in the Nepal Himalaya revealed by spirit leveling, Geophys. Res. Lett. 19, 1539–1542, 1992.
[43] P. Rochette, Inverse magnetic fabric carbonate bearing rocks, Earth Planet. Sci. Lett. 90, 229–237, 1988.
[44] D.K. Potter and A. Stephenson, Single-domain particles in rocks and magnetic fabric analysis, Geophys. Res. Lett. 15, 1097–1100, 1988.
[45] B.B. Ellwood, W. Balsam, B. Burkart, G. Long and M. Buhl, Anomalous magnetic properties in rocks containing siderite: paleomagnetic implications, J. Geophys. Res. 91, 12779–12790, 1986.
[46] P.F. Ihmlé, A. Hirt, W. Lowrie and D. Dietrich, Inverse magnetic fabric in deformed limestones of the Morcles nappe, Switzerland, Geophys. Res. Lett. 16, 1383–1386, 1989.
[47] J.P. Cogné, Strain-induced AMS in the granite of Flamanville and its effect upon TRM acquisition, Geophys. J.R. Astron. Soc. 92, 445–453, 1988.
[48] K. Zapletal, Low-field susceptibility anisotropy of some biotite crystals, Phys. Earth Planet. Inter. 63, 85–97, 1990.
[49] G.J. Borradaile, W. Keeler, C. Alford and P. Sarvas, Anisotropy of magnetic susceptibility of some metamorphic minerals, Phys. Earth Planet. Inter. 72, 215–222, 1988.
[50] R. Polino, Geologic map of Upper Imja Khola (Mt. Everest region, Eastern Nepal), scale 1:25,000, CNR–SELCA, Florence, 1981.